Universität Münster

Bachelorthesis

Constraining the Graviton Mass with PTA Data

submitted by

Kim Wassner (kwassner@uni-muenster.de)

to
Universität Münster
Institut für Theoretische Physik

First Examiner: Jun. Prof. Kai Schmitz
Second Examiner: Prof. Dr. Anna Kulesza

August 29, 2024

Abstract

The long-term observation of millisecond pulsars has for many years served as a well probed tool for gravitational wave observation. The data of these Pulsar Timing Arrays (PTAs) can be used to explore the stochastic gravitational wave background (SGWB) as well as modified theories of gravity. A key-aspect of the analysis is the Hellings-Downs Curve - the correlation of timing residuals of pulsar pairs.

This study explores modifications to the gravitational wave spectrum arising from a massive graviton in this PTA framework. First it reviews the Hellings-Downs curve of 1983[14] thus describing the characteristic correlation function of millisecond-pulsar pairs' timing residuals. Building upon this, a dispersion relation incorporating a massive graviton is introduced and the corresponding Overlap Reduction Function (ORF) is derived for this case. This reviewed result, holding an improvement for the case of autocorrelation, discussed in detail in paper [8], is then fit to timing-data from the NANOGrav collaboration. Employing Bayesian statistics, specifically the Markov Chain Monte Carlo (MCMC) method, the posterior densities and Bayes Estimator are determined for the graviton mass m_g, amplitude A, and spectral density γ of the cross-power-spectrum, including the ORF. Using the obtained cornerplot a constrain for the graviton mass was set at $m_{g,\,95\%} = 7.82 \times 10^{-24}\,\mathrm{eV}$ at 95% confidence level. A more conservative constrain was found using the probability density around the ($v_{gr} \sim c$)-limit, delivering $m_{g,\mathrm{conserv.}} = 1.07 \times 10^{-23}\,\mathrm{eV}$.

As no detectable effect of the modified ORF can be observed for even lower graviton masses, the possibility of potential lower values cannot be rules out.

This work contributes to the understanding of gravitational waves in modified gravity theories and improves the quality of boundaries set for possible modified gravity scenarios.

Declaration of Academic Integrity

I hereby confirm that this thesis, entitled *Constraining the Graviton Mass with PTA Data*, is solely my own work and that I have used no sources or aids other than the ones stated. All passages in my thesis for which other sources, including electronic media, have been used, be it direct quotes or content references, have been acknowledged as such and the sources cited. I am aware that plagiarism is considered an act of deception which can result in sanction in accordance with the examination regulations.

I consent having my thesis cross-checked with other texts to identify possible similarities and to having it stored in a database for this purpose.

I confirm that I have not submitted the following thesis in part or whole as an examination paper before.

Münster, August 29, 2024

Kim Wassner

Contents

1 Introduction **4**

2 Theoretical Foundations **5**

2.1 Metric in General Relativity and the TT-Gauge 5

2.2 Hellings-Downs-Curve in General Relativity 6

3 The Hellings Downs Curve assuming Massive Gravity **10**

3.1 Deriving the ORF for a new dispersion relation 10

3.2 Neglecting the exponential functions 13

3.3 Solving the Integral over dϕ 15

3.4 Validity of the conditions for the dϕ -Integrals 16

3.5 Solving the Integral over dx 17

4 Principles of PTA Analysis **20**

4.1 Bayesian Statistics and MCMC sampling 21

4.2 NANOGrav - Pulsar Timing Arrays 22

4.3 Implementation in PTArcade 23

5 Results and Discussion **26**

6 Outlook **28**

1 Introduction

In the field of pulsar timing array searches for gravitational waves (GW) there has been profound progress in discovering the SGWB in the nHz range. PTA collaborations measure the timing residuals for a set ("array") of galactic millisecond pulsars, in which GWs can leave an imprint in the form of a characteristic correlation pattern. The gravitational waves cause a redshift $z(t)$ in the pulsars signals which (observed over long time $t \approx 15\,\mathrm{yrs}$ [1, 26]) deliver timing residuals. The instantaneous shift of arrival times of the pulse can be set into correlation for every possible pulsar pair:

$$\langle z_a\,(t)\, z_b\,(t)\rangle = \frac{2}{3}\int_0^\infty df\;\Gamma_{ab}\,(\xi_{ab}, f)\,S_h\,(f) \tag{1}$$

where Γ_{ab} is the overlap reduction function (ORF), ξ_{ab} the angle between two pulsars a, b and $S_h\,(f)$ the spectral density (characteristic strain) or the power spectrum of the GW modes.

The following thesis will investigate the properties of Γ_{ab} in theories beyond general relativity (GR), more precisely the possibility of a nonstandard gravitational wave with a massive graviton. Adjacent works are [5, 15, 17–19, 28, 29]. The goal is to constrain the mass of the graviton m_g through inference of PTA data to a modified Hellings-Downs curve.

The assumed dispersion relation includes m_g the graviton mass, a superluminal GW phase velocity and subluminal group velocity:

$$\omega(k) = \sqrt{m_g^2 + k^2} \qquad k = |\vec{k}| \tag{2}$$

$$v_{\mathrm{ph}} = \sqrt{1 + (m_g/k)^2} \quad v_{\mathrm{group}} = 1/v_{\mathrm{ph}} \tag{3}$$

Initially, the Hellings-Downs-curve in general relativity is derived in the beginning of this paper. In Section 3 an expression for the overlap reduction function in case of massive gravity is analytically calculated. Building on the results of paper [8], the case of auto correlation Γ_{aa} is taken into consideration as well. In section 5, the derived ORF for massive gravity and the GW energy density is fitted to PTA data via Markov Chain Monte Carlo.
Including a chapter on the implemention of this bayesian statistic model, the posterior destribution then allow setting an upper bound for the mass of the graviton.

2 Theoretical Foundations

2.1 Metric in General Relativity and the TT-Gauge

In the following section some important and useful properties of the GR metric will be introduced. Following chapter two of [10], the advantages of the transverse traceless gauge will be explained. The starting point of working with gravitational waves is assuming linearized gravity, meaning that there is only a small deviation from the flat metric $\eta_{\mu\nu} = \text{diag}(-1, 1, 1, 1)$:

$$g_{\mu\nu} = \eta_{\mu\nu} + h_{\mu\nu}, \quad \|h_{\mu\nu}\| \ll 1. \tag{4}$$

$h_{\mu\nu}$ is a metric perturbation which can be written as a tensor of second order. It has sixteen components. Because not all of them reflect the physical reality some of them can be eliminated from being independent components. One is free to perform gauge transformations, which in general relativity are just coordinate transformations. A general infinitesimal coordinate transformation can be written as $x_{a'} = x_a + \xi_a$, where ξ_a is an arbitrary infinitesimal vector field.

$$h'_{\mu\nu}(x') = h_{\mu\nu}(x) - (\partial_\mu \xi_\nu + \partial_\nu \xi_\mu).$$

It is useful to introduce a trace-reversed metric perturbation given as

$$\begin{aligned} \bar{h}_{\mu\nu} &= h_{\mu\nu} - \frac{1}{2}\eta_{\mu\nu}h = h_{\mu\nu} - \frac{4}{2}h_{\mu\nu} = -h_{\mu\nu} \\ \text{with } h &= \eta^{\mu\nu}h_{\mu\nu} = h^\mu_{\ \mu} \\ \bar{h}^\mu_{\ \mu} &= -h^\mu_{\ \mu} \end{aligned}$$

If we now implement the Lorentz Gauge and thus choose ξ^μ so that

$$\partial^\nu \bar{h}_{\mu\nu} = 0, \tag{5}$$

there are four constraints on the components of $\bar{h}_{\mu\nu}$. A further transformation called the TT-gauge can now be made, preserving the Lorentz Gauge

$$\partial^\mu \partial_\mu \xi_\mu = 0$$

with $\partial^a \partial_a$ being the d´Alembertian. ξ_μ is chosen so that

$$\bar{h} = 0 \text{ meaning } \bar{h}_{\mu\nu} = h_{\mu\nu} \tag{6}$$

$$\text{and } h^{0i} = 0, \quad \text{i =1,2,3.} \tag{7}$$

Combining this with the constraints from Eq. 5 effects the zeroth and the three spatial components:

$$\partial^0 h_{00} + \partial^i h_{0i} = 0$$

This demands $h_{00} = \text{const}$. In total the TT-gauge prescribes

$$h^{0\mu} = 0, \quad h^i_i = 0(\text{traceless}), \quad \partial^j h_{ij} = 0(\text{transverse}) \tag{8}$$

This eliminates another four degrees of freedom.
Because the inital 4×4 tensor was symmetric there were ten independent components. The Lorentz- and the TT-gauge together constrain eight of them. This leaves the gravitational wave as metric perturbation just two degrees of freedom. These are present as polarization modes, h_+ and $h_\times$, showing a great advantage of the TT-gauge only containing physical, non-gauge information and exibiting the characteristic two polarization components of a gravitational wave[10].

2.2 Hellings-Downs-Curve in General Relativity

In a context of general relativity the Hellings and Downs curve is the expected correlated response of a pair of radiopulsars to a perturbation in the spacetime metric[1]. It is a function of the angle ξ_{ab} (in the calculations shortened to ξ) which is the angle between pulsars a and b as viewed from earth. The perturbation in this case is an isotropic, unpolarized stochastic background of quadrupole gravitational radiation composed of the plus (+) and cross ($\times$) polarization modes.
To derive the curve we will consider a lightbeam of a pulsar in negative $\vec{x}$-direction towards the observer in the coordinate origin. The following theoretical basis is oriented at Chapter 23 in Maggiore, M. [20]. The invariant line element is given by

$$ds^2 = -dt^2 + [\delta_{ij} + h^{TT}_{ij}(t, \vec{x})]dx^i dx^j \tag{9}$$

[1]It should be noted that the concept of the Hellings-Downs-curve is not limited to radiosignals but can also be applied in other cases of signal correlation as seen in [16].

where i, j denote the spatial coordinates, $h_{ij}^{TT}(t, \vec{x})$ the metric perturbation in the transverse traceless gauge. In the given case $i = j = x^1$ and $\delta_{ij} = 1$. Light travels along a null geodesic which is why Eq. 9 can be rearranged for dx, which allows one to Taylorexpand the term $1/\sqrt{1 + h_{xx}^{TT}}$ ($\approx 1 - \frac{1}{2} h_{xx}^{TT}$) to first order as the perturbation is relatively very small. Integrating between time of observation t_{obs} and time of emission t_{em} results in the travelled distance of pulsar a's lightpulse d_a:

$$d_a = t_{obs} - t_{em} - \frac{1}{2} \int_{t_{em}}^{t_{obs}} h_{xx}^{TT}(t', \vec{x}(t'))dt' \tag{10}$$

Using natural units the distance $d_a = \tau_a$, the travel time. In unperturbed space the time of observation t_{obs} would be given by the sum of $\tau_a + t_{em}$[2] whereas here it is given by

$$t_{obs} = d_a + t_{em} + \frac{n_a^i n_a^j}{2} \int_{t_{em}}^{t_{em}+d_a} dt'\, h_{ij}^{TT}[t', (t_{em} + d_a - t')\vec{n}_a]. \tag{11}$$

Notice that h_{xx}^{TT} has been generalized to $n_a^i n_a^j h_{ij}^{TT}$ describe a perturbed pulsar beam from arbitrary direction. A monochromatic GW in $\vec{k}$-direction can be discribed by

$$h_{ij}^{TT}(t, \vec{x}) = \mathcal{A}_{ij}(\vec{k}) \cos\left[\omega_{\mathrm{gw}}(t - \vec{k}\vec{x})\right]. \tag{12}$$

Eq. 11 can be altered to describe t'_{obs}, the observation time of the next puls, after one rotational period T_a of a millisecond pulsar.

Subtracting these observation times one can define ΔT_a and furthermore taylorexpand the dependence of t'_{obs} on $\omega_{\mathrm{gw}} T_a$ which is extremely small (typically ω_{gw} is of order $\leq 10^{-10}$). This leads to

$$\frac{\Delta T_a}{T_a} = \frac{n_a^i n_a^j \mathcal{A}_{ij}}{2(1 + \vec{k} \cdot \vec{n}_a)} [\cos(\omega_{\mathrm{gw}} t_{obs}) - \cos(\omega_{\mathrm{gw}} t_{em} - \omega_{\mathrm{gw}} T_a \vec{k} \cdot \vec{n}_a)]. \tag{13}$$

This equals to the conventional definition of $z_a(t) = -(\Delta\nu_a/\nu_a)(t) = \frac{\Delta T_a}{T_a}$ (as seen in Chapter 23 of [20]), which is the Doppler shift of pulsar a's photons.

Instead of to a monochromatic wave like in Eq. 12 one now applies the latter to a function $h_{ij}^{TT}(t, \vec{x})$ describing a SGWB - a superposition of waves of all frequencies coming from all directions.

$$h_{ij}^{TT}(t, \vec{x}) = \sum_{A=+,\times} \int_{-\infty}^{\infty} df \int d^2\vec{k}\, \tilde{h}_A(f, \vec{k}) e_{ij}^A(\vec{k}) e^{-2\pi i f(t - \vec{k}\vec{x})} \tag{14}$$

[2]Note that $x = d_a$ and $x = 0$ are defined by the position of the pulsar a and the observer repectively. They are independent of h_{ij}^{TT} because ofthe TT-Gauge.

Like shown in [16] by using Eq. 13 this results in the following.

$$z_a(t) = \sum_{A=+,\times} \int_{-\infty}^{\infty} df \int d^2\vec{k}\; \tilde{h}_A(f,\vec{k}) F_a^A(\vec{k}) e^{-2\pi i f t} \cdot \left[1 - e^{2\pi i f \tau_a \left(1+\vec{k}\cdot\vec{n}_a\right)}\right] \tag{15}$$

The sum over A includes the GW-polarizations and $\tilde{h}_A(f,\vec{k})$ is the stochastic variables. Also the "antenna pattern" functions are introduced as

$$F_a^A(\vec{k}) = \frac{n_a^i n_a^j e_{ij}^A(\vec{k})}{2\left(1+\vec{k}\cdot\vec{n}_a\right)}. \tag{16}$$

Now to correlate the redshifts of two two pulsars a and b the ensemble average is calculated given by

$$\langle z_a(t) z_b(t)\rangle = \frac{1}{2}\int_{-\infty}^{\infty} \mathrm{d}f S_h(f) \int \frac{d^2\vec{k}}{4\pi} \mathcal{K}_{ab}(f;\vec{k}) \sum_{A=+,x} F_a^A(\vec{k}) F_b^A(\vec{k}) \tag{17}$$

The term $\mathcal{K}_{ab}(f;\vec{k})$ corresponds to the sum over the term in angled brackets in Eq. 15. It can be replaced with 1 considering that these perturbation terms h can be seen as causally uncorrelated except for the term originating from $\langle h_{ij}(t,\vec{x}=0) h_{kl}(t,\vec{x}=0)\rangle$ which corresponds to 1. An extended explanation is given on page 731 in Maggiore [20].
$S_h(f) = S_h(-f)$ is the spectral density of the SGWB, which is why it can be replaced with the one-sided spectrum:

$$\langle z_a(t) z_b(t)\rangle = \int_0^{\infty} \mathrm{d}f S_h(f) \cdot C(\xi) \tag{18}$$

For reasons of a fitting normalization of the Hellings Downs curve one can introduce a factor of β to the ensemble average $\langle z_a(t) z_b(t)\rangle$ and revoke it with a factor of $1/\beta$ infront of $C(\xi)$ which we call the overlap reduction function for GR Γ_{ab}^0:

$$\Gamma_{ab}^0 = \frac{1}{\beta} C(\xi_{ab}) = \frac{1}{\beta}\frac{1}{4\pi}\int \mathrm{d}^2\vec{k} F_a^A(\vec{k}) F_b^A(\vec{k}) = \frac{1}{4\pi}\int \mathrm{d}^2\vec{k} \frac{n_a^i n_a^j e_{ij}^+(\vec{k}) n_b^k n_b^l e_{ij}^+(\vec{k})}{2(1+\vec{k}\cdot\vec{n}_a)2(1+\vec{k}\cdot\vec{n}_b)}. \tag{19}$$

To now compute $C(\xi)$ one needs to specify the variables and coordinates. Still using the TT-gauge, it is given that $h_i^i = 0$ and $\partial^j h_{ij} = 0$. Further $\vec{k}(\theta,\phi)$ is the propagation direction of the gravitational wave in spherical coordinates.

$$\vec{k}_{(\theta,\phi)} = (\sin\theta\cos\phi, \sin\theta\sin\phi, \cos\theta)^T$$

The perpendicular polarization tensors (to each other and $\vec{k}$) are given by

$$e^{+}_{ij}(\vec{k}) = u_i u_j - v_i v_j \tag{20}$$

$$e^{\times}_{ij}(\vec{k}) = u_i v_j + v_i u_j \tag{21}$$

$$\longrightarrow \vec{u} = (\sin\phi, -\cos\phi, 0) \quad \text{and} \quad \vec{v} = (\cos\theta\cos\phi, \cos\theta\sin\phi, -\sin\theta)$$

and further we choose $\vec{n}_a = (0,0,1)$ and $\vec{n}_b = (\sin\xi, 0, \cos\xi)$ to be the pulsars directional vectors which stand to each other at an angle ξ.

The following calculations are extendedly done in Appendix A (**Simplification of the Hellings and Downs curve integral**). It is shown that all $\times$-polarization terms vanish and that the correlation-integral can be written as follows:

$$C(\xi) = \frac{1}{16\pi}\int \mathrm{d}^2\vec{k}\,\frac{\sin^2\theta(\sin\xi\cos\theta\cos\phi - \cos\xi\sin\theta)^2 - \sin^2\xi\sin^2\phi}{(1+\cos\theta)(1+\cos\xi\cos\theta+\sin\xi\sin\theta\cos\phi)} \tag{22}$$

$$= \frac{1}{16\pi}\int_{-1}^{1}\sin\theta\mathrm{d}\theta\int_0^{2\pi}(1-\cos\theta)\cdot F_2^{+}(\vec{k}) \qquad \to x = \cos\theta \tag{23}$$

$$= \frac{1}{16\pi}\int_{-1}^{1}\mathrm{d}x\,(1-x)\cdot(I_1+I_2), \tag{24}$$

Hereby one defining two integrals to solve for the $\mathrm{d}\phi$ integration

$$I_1 = \frac{1}{2}\int_0^{2\pi}\mathrm{d}\phi\,\frac{1}{2}(1-\cos\xi\cos\theta-\sin\xi\sin\theta\cos\phi)$$

$$I_2 = -\frac{1}{2}\int_0^{2\pi}\mathrm{d}\phi\frac{2\sin^2\xi\sin^2\phi}{(1+\cos\xi\cos\theta+\sin\xi\sin\theta\cos\phi)}.$$

The first integral I_1 is trivial and I_2 can be calculated using contour integration which is done in Appendix A (from Eq. A.12).Notice that $x \equiv \cos\theta$. Receiving the following results,

$$I_1 = \pi(1-\cos\xi\cdot x) \tag{25}$$

$$I_2 = \frac{-2\pi(1\mp\cos\xi)}{(1\pm x)} \tag{26}$$

we can return to Eq. 24. Considering the signs of I_2, meaning the bottom sign is valid when x

is between $[-1, -\cos\xi]$ and the top sign for x between $[-\cos\xi, 1]$ (cf. [16]) makes

$$C(\xi) = \frac{1}{16}\left[\int_{-1}^{1}(1-x\cos\xi)(1-x)\mathrm{d}x \right. \\ \left. - \int_{-1}^{-\cos\xi}\frac{2(1+\cos\xi)(1-x)}{(1-x)}\mathrm{d}x - \int_{-\cos\xi}^{1}\frac{2(1-\cos\xi)(1-x)}{1+x}\mathrm{d}x\right]. \tag{27}$$

Eventually after these basic integrals the Hellings Downs Curve is found as as function of purely the angle between the two pulsars [14]. Multiplying by three gives us the normalisation also used in paper [8]

$$\frac{1}{\beta}C(\xi) = \frac{1}{2} - \frac{1}{4}\left(\frac{1-\cos\xi}{2}\right) + \frac{3}{2}\left(\frac{1-\cos\xi}{2}\right)\ln\left(\frac{1-\cos\xi}{2}\right). \tag{28}$$

Being precise this is only the Hellings Downs curve under the condition $a \neq b$. When taking into account the case of $\xi_{aa} = 0$ one should introduce a Kronecker-delta as argued in chapter 5 of paper [8] to receive the right expression for the ORF:

$$\Gamma^0_{ab} = (1+\delta_{ab})\left[\frac{1}{2} - \frac{1}{4}\left(\frac{1-\cos\xi}{2}\right) + \frac{3}{2}\left(\frac{1-\cos\xi}{2}\right)\ln\left(\frac{1-\cos\xi}{2}\right)\right]. \tag{29}$$

The explanation is that the derived auto correlation coefficient $\Gamma_{a,a}$ equals to twice the zero-angle-limit of $\Gamma_{ab}(\xi \to 0)$. Now, when looking at the value of the C for an angle of $\xi_{aa} = 0$ we are only left with $1/2$ from the original function and a factor of 2, which then gives the correlator a value of 1.

3 The Hellings Downs Curve assuming Massive Gravity

3.1 Deriving the ORF for a new dispersion relation

Orienting this chapter towards the paper of Qiuyue Liang and Mark Trodden [19] the calculations will use the $(+---)$ signature convention. When assuming a massive graviton, one needs to apply a different dispersion relation:

$$\omega(|\vec{k}|) = \sqrt{m_g^2 + |\vec{k}|^2} \tag{30}$$

Here m_g is the graviton mass. The group-velocity is subluminal with

$$v_{gr} = \frac{1}{\sqrt{1+(m_g/|\vec{k}|)^2}} = \frac{|\vec{k}|}{k_0} \equiv A \tag{31}$$

The frequency ω of the GW with $c = 1$ will now be called $\omega = k_0$. As $E = \hbar\omega$ and the momentum is $\vec{p} = \hbar\vec{k}$, using the energy-momentum relation (length of the four-momentum)

$$E^2 - m^2 = \vec{p}^2, \tag{32}$$

results in,

$$k_0^2 - m^2 = |k_\mu|^2. \tag{33}$$

We call $\hat{\Omega} = (\sin\theta\cos\phi, \sin\theta\sin\phi, \cos\phi)$ the unit vector of the spatial direction of the GW. The four-vector $\vec{k} = k_\mu$ is then ($k_0 = \omega/c$)

$$k_\mu = \begin{pmatrix} k_0 \\ |\vec{k}|\sin\theta\cos\phi \\ |\vec{k}|\sin\theta\sin\phi \\ |\vec{k}|\cos\theta \end{pmatrix} = k_0\left(1, \frac{|\vec{k}|}{k_0}\hat{\Omega}\right) \tag{34}$$

The Klein-Gordon equations of motion for a massive graviton are given and solved by

$$(\Box - m^2)h_{\mu\nu}(x) = 0 \Leftrightarrow k_0^2 = |\vec{k}|^2 + m^2 \tag{35}$$

which is imposed in the following by a deltafunction in the massive spin-two metric perturbation tensor

$$h_{\mu\nu}(\vec{x}) = \frac{1}{2\pi}\int d^4k \frac{2\delta(|\vec{k}|^2 - (k_0^2 - m^2))}{|\vec{k}|} e^{ikx} h_{\mu\nu}(k). \tag{36}$$

Expressing this as shown in the Appendix A of [15] gives

$$h_{\mu\nu}(\vec{x}) = \int_{-\infty}^{\infty}\int_{\text{sky}} e^{2\pi i f(t - \frac{|\vec{k}|}{k_0}\hat{\Omega}\vec{x}))} h_{\mu\nu}(f, \frac{|\vec{k}|}{k_0}\hat{\Omega})\ \mathrm{d}f\ \mathrm{d}^2\hat{\Omega}. \tag{37}$$

What has been done, is that $h_{\mu\nu}$ was expanded as a plane wave in locally flat spacetime

$$h_{\mu\nu}(\vec{x}) = \frac{1}{2\pi}\int h_{\mu\nu}(\vec{k}) \cdot e^{i\vec{k}\vec{x}} \widetilde{\mathrm{d}\vec{k}} \tag{38}$$

defining $\widetilde{\mathrm{d}\vec{k}}$ as

$$\widetilde{\mathrm{d}\vec{k}} \equiv 2c\frac{\delta(|\vec{k}|^2 - |\vec{k_0}|^2)}{|\vec{k}|}\mathrm{d}\vec{k}. \tag{39}$$

Up till here $\vec{k}$ is still a four-vector and can be split up into frequency $2\pi f = \omega$ and a spatial three-vector (Eq. 34), such that $\mathrm{d}\vec{k} = |\vec{k}|^2 \mathrm{d}|\vec{k}| \mathrm{d}^2\hat{\Omega}$. So we now integrate over a 2-sphere $\mathrm{d}^2\hat{\Omega}$ with a non negative radius $|\vec{k}|$. Further, as in paper [15], it was used that for a continuously differentiable function $g(x)$ it can be said that $\delta(g(x)) = \sum_i \frac{\delta(x-x_i)}{|g'(x_i)|}$, where $g' = 2|\vec{k_0}|$.

$$h_{\mu\nu} = \frac{1}{2\pi} \int_{-\infty}^{\infty} \int_{\mathrm{S}^2} \int_{0}^{\infty} h_{\mu\nu}(\omega, \vec{k}) \cdot e^{i(\omega t - \vec{k}\vec{x})} \times \frac{1}{|\vec{k_0}|} \delta\left(|\vec{k}| - |\vec{k_0}|\right) |\vec{k}| \, \mathrm{d}|\vec{k}| \, \mathrm{d}^2\hat{\Omega} \, \mathrm{d}\omega \tag{40}$$

One can now solve the integral simply via the delta function ($|\vec{k}| = |\vec{k_0}|$) to receive

$$h_{\mu\nu}(t, \vec{x}) = \frac{1}{2\pi} \int_{-\infty}^{\infty} \int_{\mathrm{S}^2} h_{\mu\nu}(\omega, \vec{k}) e^{i(\omega t - \vec{k}\vec{x})} \, \mathrm{d}\omega \, \mathrm{d}^2\hat{\Omega} \tag{41}$$

Eventually, one can see that $\widetilde{\mathrm{d}\vec{k}}$ is given by

$$\widetilde{\mathrm{d}\vec{k}} = \mathrm{d}\omega \, \mathrm{d}^2\hat{\Omega}. \tag{42}$$

Like this, one arrives at Eq. 37, when considering the definition of the $\vec{k}$ vector and noting that $\mathrm{d}\omega/2\pi = \mathrm{d}f$. The $h_{\mu\nu}(f, \frac{|\vec{k}|}{k_0}\hat{\Omega})$ in Eq. 37 can furthermore be expressed as a sum over its polarization tensors.

$$\sum_i h^{(i)} \epsilon^{(i)}_{\mu\nu} \tag{43}$$

At this point the same steps are followed as for the correlation of the massless timing residuals. Due to a change in the measured pulsar frequency there will be a residual in the measured pulse arrival time. The light path $s^\mu = \nu\hat{p}$ from pulsar to earth with frequency ν ($\vec{x}_{\mathrm{Earth}} = 0$ and $\vec{x}_{\mathrm{Pulsar}} = L\hat{p}$) once again follows a null geodesic. This helps to define

$$h_{\mu\nu}\left(t - \frac{|\vec{k}|}{k_0}\hat{\Omega} \cdot \vec{x}\right) = \int_{-\infty}^{\infty} \mathrm{d}f e^{i2\pi f(t - \frac{|\vec{k}|}{k_0}\hat{\Omega}\cdot\vec{x})} h_{\mu\nu}(f, \frac{|\vec{k}|}{k_0}\hat{\Omega}) \tag{44}$$

as the propagation of a metric perturbation in the direction of $\hat{\Omega}$ as well as the redshift z as a function of frequency (as seen in pages 7-8 of [19])

$$z(f, \hat{\Omega}) = \frac{\nu_0 - \nu(t)}{\nu_0} = \left(e^{-i2\pi f L(1 + \frac{|\vec{k}|}{k_0}\hat{\Omega}\hat{p})} - 1\right) \sum_i h^{(i)}\left(f, \frac{|\vec{k}|}{k_0}\hat{\Omega}\right) F^{(i)}(\hat{\Omega}). \tag{45}$$

$F^{(i)}(\hat{\Omega})$ is the antenna- or receiving function defined as

$$F^{(i)}(\hat{\Omega}) = -\frac{\hat{p}^\mu \hat{p}^\nu}{2(1+\frac{|\vec{k}|}{k_0}\hat{\Omega}\hat{p})}\epsilon^{(i)}_{\mu\nu} + \frac{\hat{p}_\mu}{2}\epsilon^{(i)}_{0\mu}. \tag{46}$$

Since the goal is to detect the SGWB, i.e. GW arriving from all directions, the relevant quantity is the total redshift

$$\tilde{z}(f) = \int_{\mathrm{S}^2} \mathrm{d}f \; z(f, \hat{\Omega}) \tag{47}$$

and with it its two-point correlation function $\langle \tilde{z}(f)\tilde{z}(f)\rangle$. As in [26] it will be assumed that the frequency dependence of this power spectrum is independent of any spatial correlations which enables the separation into two parts: $\langle h^{(i)2}\rangle$, related to the energy density and the shape of the signal, the overlap reduction function denoted by $\Gamma(|f|)$. Till now $\Gamma(|f|)$ is defined by

$$\Gamma(|f|) = \beta_T \sum_i \int_{\mathrm{S}^2} \mathrm{d}^2\hat{\Omega}\, (e^{i2\pi f L_1(1+\frac{|\vec{k}|}{k_0}\hat{\Omega}\hat{p}_1)} - 1)(e^{-i2\pi f L_2(1+\frac{|\vec{k}|}{k_0}\hat{\Omega}\hat{p}_2)} - 1) F_1^{(i)}(\hat{\Omega}) F_2^{(i)}(\hat{\Omega}) \tag{48}$$

3.2 Neglecting the exponential functions

The following sections talks about why the exponential terms can be neglected in the ORF for massive gravity. For once, as seen in chapter 23.3 of [20] the four terms resulting from the exponential brackets can be backtraced to the ensemble averages. Leaving out the fourth term, which is just one, they are:

$$\langle h_{ij}((t-\tau_1), \vec{p}_1) h_{kl}(t, \vec{x}_{\mathrm{Earth}} = 0)\rangle \tag{49}$$

$$\langle h_{ij}(t, \vec{x}_{\mathrm{Earth}} = 0) h_{kl}((t-\tau_2), \vec{p}_2)\rangle \tag{50}$$

$$\langle h_{ij}((t-\tau_1), \vec{p}_1) h_{kl}(t-\tau_2, \vec{p}_2)\rangle \tag{51}$$

These are terms at different space points. These are each uncorrelated since T= O(10)yr of GW is compably small to the time τ it takes the pulse to go from the pulsar to the observer. Looking at the closest millisecond pulsar which is a distance $L = 156$pc away, and the minimum f in the PTA frequency range is $(\approx 3 \cdot 10^{-9})$Hz. The smallest fL is then of order 50 but typically 300. Thus the terms are rapidly oscillating exponentials that contribute negligibly to the integral over $\mathrm{d}f$.

In [19] the massless and the stationary limit are looked at. It is observed that Γ includes one slow oscillation mode $2\pi\frac{|\vec{k}|}{k_0}$ and one fast one with frequency 2π. When intgrating over the di-

rection vector of the GW $\hat{\Omega}$ the slow oscillation causes a damping behaviour. For $\frac{|\vec{k}|}{k_0} \Rightarrow 1$ both frequencies are 2π so Γ damps rapidly for $fL > 10$ (as seen above, this is the absolute minimum order relevant for PTA observation) and so quickly reaches analog Hellings-Downs curve.
For $\frac{|\vec{k}|}{k_0} \Rightarrow 0$ the slow oscillation mode does not contribute. The fast oscillation mode is independent of the angle between the pulsars and therefore does not contribute to the angular dependence of Γ, so the GR Hellings-Downs curve is a good approximation as well. For an angle $\xi = \pi/8$ the numeric difference of the overlap reduction function value Γ between $\frac{|\vec{k}|}{k_0} = 0.9$ and $\frac{|\vec{k}|}{k_0} = 1$ is less than 5%, as shown by Q.Liang & M.Trodden on p.12 in [19] for the relevant frequencies and distances.

Hence one arrives at the overlap reduction function Γ_{ab}

$$\Gamma_{ab} = \beta_T \sum_{i=\pm 2} \int \mathrm{d}\hat{\Omega} F_1^{(i)}(\hat{\Omega}) \cdot F_2^{(i)}(\hat{\Omega}). \tag{52}$$

The factor β_T is for normalization. The receiving functions are defined in Eq. 46 - note that its second term is zero because $\epsilon_0^{\pm}$ is zero. With $\epsilon_{\mu\nu}^{\pm 2} = \epsilon_\mu^{\pm} \epsilon_\nu^{\pm}$ there are two relevant polarization modes. They are defined by

$$\epsilon_\mu^{\pm}(k) = \frac{1}{\sqrt{2}}(0, \cos\theta\cos\phi, \mp i\sin\phi, \cos\theta\sin\phi \pm i\cos\phi, -\sin\theta) \tag{53}$$

The pulsar directional vectors in the following are $\vec{p}_1 = (1,0,0,1)^T$ and $\vec{p}_2 = (1, \sin\xi, 0, \cos\xi)^T$, the propagation direction of the GW is $\vec{\Omega}$ and $|\vec{k}|/k_0$ is the group velocity v_{gr}. This is also visualised in Figure 1.

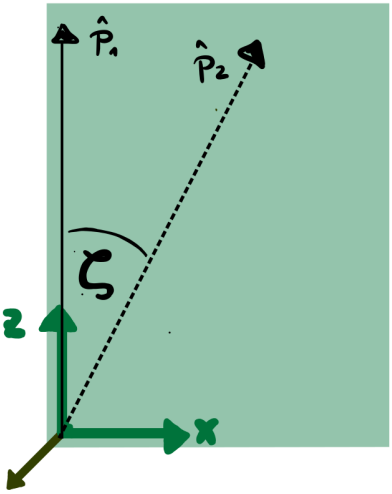

Figure 1: Two pulsars $\hat{p}_{1,2}$ at angle ξ ($\rightarrow \zeta$) in the x-z-plane with the observer at the origin.

3.3 Solving the Integral over dϕ

The relevant terms for Γ_{ab} are

$$
\begin{aligned}
(1 + v_{\rm gr}\vec{\Omega}\vec{p}_1) &= 1 + v_{\rm gr}\cos\theta \\
(1 + v_{\rm gr}\vec{\Omega}\vec{p}_2) &= 1 + v_{\rm gr}\cos\theta \\
\vec{p}_1^{\,\mu}\epsilon_\mu^{\,+}\ \vec{p}_1^{\,\nu}\epsilon_\nu^{\,+} &= \frac{\sin^2\theta}{2} \\
\vec{p}_2^{\,\mu}\epsilon_\mu^{\,+}\ \vec{p}_2^{\,\nu}\epsilon_\nu^{\,+} &= \frac{1}{2}\left(\sin\xi(\cos\theta\cos\phi - i\sin\phi) - \cos\xi\sin\theta\right)^2 \\
\vec{p}_1^{\,\mu}\epsilon_\mu^{\,-}\ \vec{p}_1^{\,\nu}\epsilon_\nu^{\,-} &= \frac{\sin^2\theta}{2} \\
\vec{p}_2^{\,\mu}\epsilon_\mu^{\,-}\ \vec{p}_2^{\,\nu}\epsilon_\nu^{\,-} &= \frac{1}{2}\left(\sin\xi(\cos\theta\cos\phi + i\sin\phi) - \cos\xi\sin\theta\right)^2 .
\end{aligned}
$$

The overlap reduction function is thus given as

$$\Gamma_{ab} = \beta_T \sum_{i=\pm 2}\int \mathrm{d}\hat{\Omega} F_1^{(i)}(\hat{\Omega})\cdot F_2^{(i)}(\hat{\Omega}) \tag{54}$$

$$
\begin{aligned}
&= \frac{\beta_T}{4}\int \mathrm{d}\hat{\Omega}\frac{\sin^2\theta}{2\left(1 + v_{\rm gr}\cos\theta\right)} \\
&\times \frac{\left[\cos^2\xi\sin^2\theta - 2\cos\theta\sin\theta\cos\xi\sin\xi\cos\phi + \sin^2\xi(\cos^2\theta\cos^2\phi - \sin^2\phi)\right]}{1 + v_{\rm gr}(\cos\theta\cos\xi + \cos\phi\sin\theta\sin\xi)}
\end{aligned} \tag{55}
$$

From now on $1 + v_{\rm gr}(\cos\theta\cos\xi + \cos\phi\sin\theta\sin\xi) = a + b\cos\theta$ and we substitute $x = \cos\theta$ while $\mathrm{d}\hat{\Omega} = \mathrm{d}\theta\mathrm{d}\phi\sin\theta$. So eventually we can divide the integral into three parts in which the $C_{1,2,3}$ are independent of ϕ

$$\Gamma_{ab} = \frac{\beta_T}{4}\int_{-1}^{1}\mathrm{d}x\frac{1-x^2}{2(1 + v_{\rm gr}\,x)}\int_0^{2\pi}\mathrm{d}\phi\frac{C_1}{a + b\cos\phi} - \frac{C_2\cos\phi}{a + b\cos\phi} + \frac{C_3\cos^2\phi}{a + b\cos\phi} \tag{56}$$

with

$$C_1 = \cos^2\xi(1 - x^2) - \sin\xi \tag{57}$$

$$C_2 = -2x\sqrt{1 - x^2}\cos\xi\sin\xi \tag{58}$$

$$C_3 = \sin^2\xi(1 + x^2). \tag{59}$$

First solving the integrals over $d\phi$ and noting

$a = v_{\rm gr}x\cos\xi$

$b = v_{\rm gr}\sqrt{1 - x^2}\sin\xi$ and

$a^2 - b^2 = 1 + 2v_{\rm gr}x\cos\xi + v_{\rm gr}^2(x^2 - \sin^2\xi) = (v_{\rm gr}x = \cos\xi)^2 + (1 - v_{\rm gr}^2)(1 - \cos^2\xi)$

we receive

$$I_1 = 2\pi C_1 \frac{1}{\sqrt{a^2 - b^2}} \tag{60}$$

$$I_2 = 2\pi C_2 \left(\frac{1}{b} - \frac{a}{b\sqrt{a^2 - b^2}} \right) \tag{61}$$

$$I_3 = 2\pi C_3 \left(\frac{a^2}{b^2\sqrt{a^2 - b^2}} - \frac{a}{b^2} \right) \tag{62}$$

as solutions.

3.4 Validity of the conditions for the dϕ -Integrals

The two conditions of the integrals' solutions are

$$\left| \frac{a + \sqrt{a^2 - b^2}}{b} \right| \geq 1 \quad \& \quad \left| \frac{a - \sqrt{a^2 - b^2}}{b} \right| < 1, \tag{63}$$

where a and b have been defined as

$$a = 1 + v_{\mathrm{gr}}\, x \cos\xi, \quad b = v_{\mathrm{gr}} \sqrt{1 - x^2} \sin\xi.$$

Beforehand x was substituted from $\cos\theta$ and therefore ranges from $[-1, 1]$. The angle ξ describing the angular separation of pulsars on the firmament goes from $[0, \pi]$, the Cosine of ξ takes values from $[1, -1]$ and the Sine takes values between $[0, 1]$. The group velocity $v_{\mathrm{gr}} = |\vec{k}|/k_0$ is a posive parameter.

Conclusively this means that a, as well as b are positive definite and the conditions can be rearranged to

$$a - b \geq -\sqrt{a^2 - b^2} \qquad a + b < \sqrt{a^2 - b^2}. \tag{64}$$

This is possible to be written without absolutes as it can be shown that $a > b$ (and $a^2 > b^2$) is always given. The maximal value of b is v_{gr} (taking $x = 0$ and $\sin\xi = 1$) and the minimal value

of a is 1. The first condition in Eq. 64 is then true. One can look for a solution in which $a = b$:

$$\begin{aligned}
& 1 + v_{\rm gr}\, x \cos\xi = v_{\rm gr}\sqrt{1-x^2}\sin\xi \\
\Leftrightarrow\quad & v_{\rm gr}^2 x^2 + 2\, v_{\rm gr} x \cos\xi + 1 - v_{\rm gr}^2 \sin^2\xi = 0 \\
\Rightarrow\quad & x = -\frac{\cos\xi}{v_{\rm gr}} \pm \sqrt{\frac{\cos^2\xi}{v_{\rm gr}^2} - \frac{1}{v_{\rm gr}^2} + \sin^2\xi} \\
\Leftrightarrow\quad & x = -\frac{\cos\xi}{v_{\rm gr}} \pm \frac{\sin\xi}{v_{\rm gr}}\sqrt{v_{\rm gr}^2 - 1}
\end{aligned}$$

This shows that there are only real solutions for x if $v_{\rm gr} \geq 1$. But if $v_{\rm gr}$ is supposed to stay inside the bounds of $(0, 1)$ assuring that $\frac{v}{c} < 1$ for a massive graviton, then a is always larger than b. The second condition in Eq. 64 can be rewritten as

$$(a-b)^2 < a^2 - b^2 \quad \Leftrightarrow \quad 2b^2 < 2ab \quad \Leftrightarrow \quad b < a, \tag{65}$$

which is therefore true.

3.5 Solving the Integral over dx

We will now write Eq. 56 in the Form:

$$\begin{aligned}
\Gamma_{ab} &= \frac{\beta_T\, \pi}{4} \int_{-1}^{1} {\rm d}x\; \chi(x) \\
&= \frac{\beta_T\, \pi}{4} \int_{-1}^{1} {\rm d}x\; \frac{1-x^2}{1+v_{\rm gr}\, x} \left[\frac{C_1}{\sqrt{a^2-b^2}} + C_2 \left(\frac{1}{b} - \frac{a}{b\sqrt{a^2-b^2}} \right) + C_3 \left(\frac{a^2}{b^2\sqrt{a^2-b^2}} - \frac{a}{b^2} \right) \right]
\end{aligned}$$

with

$$\begin{aligned}
a &= 1 + v_{\rm gr} x \cos\xi \qquad & C_1 &= \cos^2\xi(1-x^2) - \sin\xi \\
b &= v_{\rm gr}\sqrt{1-x^2}\sin\xi \qquad & C_2 &= -2x\sqrt{1-x^2}\cos\xi\sin\xi \\
& & C_3 &= \sin^2\xi(1+x^2)
\end{aligned}$$

$$\sqrt{a^2-b^2} = \sqrt{(v_{\rm gr}\, x + \cos\xi)^2 + (1-v_{\rm gr}^2)(1-\cos\xi^2)}.$$

The Integrand $\chi(x)$ can be simplied to just

$$\begin{aligned}
\chi(x) &= \frac{1}{(1+v_{\rm gr}\, x)} \\
&\times \left[\frac{1-x^2}{v_{\rm gr}^2} + \frac{x^3\cos\xi - 3x\cos\xi}{v_{\rm gr}} + \frac{1}{\sqrt{a^2-b^2}} \left(x^2 - 1 + 2\cos^2\xi + \frac{4x\cos\xi}{v_{\rm gr}} + \frac{1+x^2}{v_{\rm gr}^2} \right) \right].
\end{aligned}$$

Using `mathematica` this can be integrated under the assumption that $v_{\rm gr} \in (0, 1)$ and $\cos\xi \in [-1, 1)$. It proved helpful to define $(\cos\xi = u)$ and $(\sin\xi = \sqrt{1-u^2})$. The limits $x = 1$

and $x = -1$ can then be inserted seperately and the terms subtracted. When working with `mathematica` one has to convert the following factors in the `simplified` expression:

- $\operatorname{arctanh}(v_{\rm gr}) \to \frac{1}{2}\ln\frac{(1+v_{\rm gr})}{(1-v_{\rm gr})}$
- $\sqrt{(v_{\rm gr}\cos\xi - 1)^2} \to (1 - v_{\rm gr}\cos\xi)$
- $\sqrt{1-\cos\xi}\sqrt{-2+v_{\rm gr}^2(1+\cos\xi)} \to \quad -\sqrt{(1-\cos\xi)(-2+v_{\rm gr}^2(1+\cos\xi))}.$

Rearranging the expression, while sorting the terms after their logarithm-dependency leeds to

$$\int_{-1}^{1}\chi(x)\mathrm{d}x = \frac{1}{3v_{\rm gr}^5}\left[X + Y\ln\left(\frac{1+v_{\rm gr}}{1-v_{\rm gr}}\right) + Z\ln\frac{N}{D}\right]$$

where

$$X = -10v_{\rm gr}^3\cos\xi + 12v_{\rm gr}\cos\xi + 6v_{\rm gr}$$

$$Y = \frac{-3(1+2v_{\rm gr}^2(1-2\cos\xi)+v_{\rm gr}^4(-1+2\cos^2\xi))}{\sqrt{(1-\cos\xi)(-2+v_{\rm gr}^2(1+\cos\xi))}} - 6(1+\cos\xi - v_{\rm gr}^2(3\cos\xi - 1))$$

$$Z = \frac{-3(1+2v_{\rm gr}^2(1-2\cos\xi)+v_{\rm gr}^4(-1+2\cos^2\xi))}{\sqrt{(1-\cos\xi)(-2+v_{\rm gr}^2(1+\cos\xi))}}$$

$$N = 1 + v_{\rm gr} - v_{\rm gr}^2 - \cos\xi - v_{\rm gr}\cos\xi + v_{\rm gr}^2\cos^2\xi - (1 - v_{\rm gr}\cos\xi)\sqrt{(1-\cos\xi)(-2+v_{\rm gr}^2(1+\cos\xi))}$$

$$D = 1 - v_{\rm gr} - v_{\rm gr}^2 - \cos\xi + v_{\rm gr}\cos\xi + v_{\rm gr}^2\cos^2\xi - (1 + v_{\rm gr}\cos\xi)\sqrt{(1-\cos\xi)(-2+v_{\rm gr}^2(1+\cos\xi))}.$$

Due to the agreement of the coefficient term Z and the first part of Y, the latter will be combined with Z and its corresponding logarithm.
Eventually what is left to do is simplify the term $\ln\frac{(1+v_{\rm gr})N}{(1-v_{\rm gr})D}$.
In the first step it is expedient to multiply N and D with

$$\times\left[1 + v_{\rm gr} - v_{\rm gr}^2 - \cos\xi - v_{\rm gr}\cos\xi + v_{\rm gr}^2\cos^2\xi + (1 + v_{\rm gr}\cos\xi)\sqrt{(1-\cos\xi)(-2+v_{\rm gr}^2(1+\cos\xi))}\right].$$

Simplified the numerator and denominator become

$$N = -\sin^2\xi\left[1 + 2v_{\rm gr}^2 + v_{\rm gr}^4\cos 2\xi - \sqrt{8 - 2v_{\rm gr}^2 - 8\cos\xi + 2v_{\rm gr}^2\cos 2\xi}(-v_{\rm gr} - 4v_{\rm gr}^2\cos\xi + v_{\rm gr}^3\cos\xi)\right]$$
$$D = \sin^2\xi(v_{\rm gr} - 1)(1 + v_{\rm gr})^3,$$

which can then be multiplied by $(1+v_{\rm gr})$ and $(1-v_{\rm gr})$ respectively. The result is

$$\frac{[1+2v_{\rm gr}^2+v_{\rm gr}^4\cos 2\xi-\sqrt{8-2v_{\rm gr}^2-8\cos\xi+2v_{\rm gr}^2\cos 2\xi}(-v_{\rm gr}-4v_{\rm gr}^2\cos\xi+v_{\rm gr}^3\cos\xi)]}{(1-v_{\rm gr})(1-v_{\rm gr})(1+v_{\rm gr})(1+v_{\rm gr})}=$$
$$\frac{1+2v_{\rm gr}^2(1-2\cos\xi)-v_{\rm gr}^4(1-2\cos^2\xi)-2v_{\rm gr}(1-v_{\rm gr}^2\cos\xi)\sqrt{(1-\cos\xi)(-2+v_{\rm gr}^2(1+\cos\xi))}}{(v_{\rm gr}^2-1)^2}.$$

Eventually, when setting $\beta_T = 6/8\pi$ the ORF for massive gravity and different pulsars ($a \neq b$) ensues as:

$$\Gamma_{ab} = \frac{1}{16v_{\rm gr}^5}\left(X + Y\ln\left(\frac{1+v_{\rm gr}}{1-v_{\rm gr}}\right) + Z\ln Q\right) \tag{66}$$

$$X = -10v_{\rm gr}^3\cos\xi + 12v_{\rm gr}\cos\xi + 6v_{\rm gr}$$

$$Y = -6(1+\cos\xi - v_{\rm gr}^2(3\cos\xi - 1))$$

$$Z = \frac{-3(1+2v_{\rm gr}^2(1-2\cos\xi)-v_{\rm gr}^4(1-2\cos^2\xi))}{\sqrt{(1-\cos\xi)(-2+v_{\rm gr}^2(1+\cos\xi))}}$$

$$Q = \frac{1+2v_{\rm gr}^2(1-2\cos\xi)-v_{\rm gr}^4(1-2\cos^2\xi)-2v_{\rm gr}(1-v_{\rm gr}^2\cos\xi)\sqrt{(1-\cos\xi)(-2+v_{\rm gr}^2(1+\cos\xi))}}{(v_{\rm gr}^2-1)^2}$$

Again it is important to look at the case of $a = b$. The analyis for the case of autocorrelation was done by setting $a = b$ right at the beginning (cf. Eq. 48). One arrives at

$$\Gamma_{aa}(f) = \frac{\beta_T}{2}\int_0^\pi {\rm d}\theta = \frac{\sin^5\theta\sin^2[\pi f L_a(1+v_{\rm gr}\cos\theta)]}{(1+v_{\rm gr}\cos\theta)} \tag{67}$$

where L_a is the pulsar distance and f the GW frequency. This integral can be solved analytically and details on the method can be found in paper [8]. Expanding the solution of Eq. 67 in inverse powers of fL_a and including the next-to-leading order terms' contribution to Γ_{aa} results in

$$\Gamma_{aa}(f) = \frac{1}{2v_{\rm gr}^5}\left[6v_{\rm gr} - 4v_{\rm gr}^3 + 3(v_{\rm gr}^2-1)\ln\left(\frac{1+v_{\rm gr}}{1-v_{\rm gr}}\right)\right]. \tag{68}$$

Remembering the group velocity reads

$$v_{\rm gr} = \frac{1}{\sqrt{1+(\frac{m_g}{k})^2}} = \sqrt{1-\left(\frac{f_g}{f}\right)^2} \tag{69}$$

with $k = |\vec{k}|$, $f_g = m_g/(2\pi)$ and $2\pi f = \sqrt{m_g^2 + k^2}$. For massive gravity the zero-angle-limit of Eq. 66 was found to have twice the value of the zero-angle-limit of Γ_{ab}:

$$\lim_{\xi_{ab}\to 0^+} \Gamma^{\text{mass}}_{\text{a}\neq\text{b}}(\xi_{ab}, f) = \frac{1}{2}\Gamma_{aa}(f). \tag{70}$$

This is just the same as in the case of GR where one finds a prefactor of two for $a = b$[8]. The following Figure 2 shows this as well. The ORF from Eq. 66 and Eq. 68 - the autocorrelation coefficients - are plotted, as well as the GR Hellings Downs Curve for comparison. The influence on the curve is the most severe for seperation angles close or equal to zero. Thus one can observe the importance of the autocorrelation function.

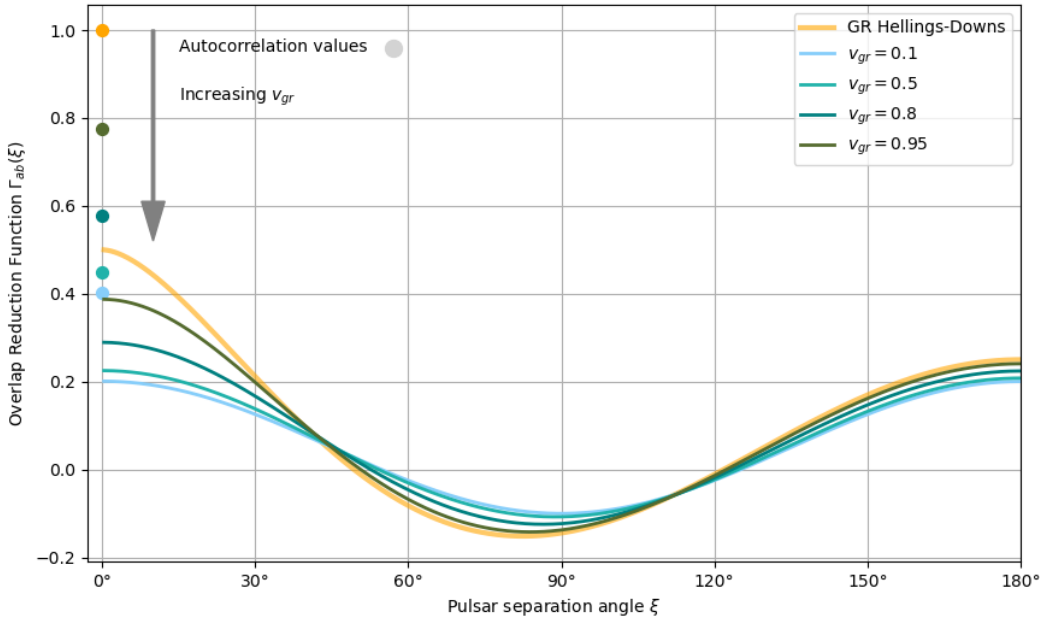

Figure 2: The ORF for different values of the group velocity v_{gr} and in orange the Hellings Downs Curve for $v_{gr} = c$. The minimum is shifts slightly towards larger angles and the ORF correlation values lie in a smaller range for decreasing v_{gr}. The marks at seperation angle of zero degrees show the values of the autocorrelation coefficient Γ_{aa} [8].

4 Principles of PTA Analysis

This sections purpose is to provide a more detailed understanding of the method of pulsar-timing and the statistic tools which are needed to constrain the graviton mass.

4.1 Bayesian Statistics and MCMC sampling

In order to combine the data of NANOGravs Pulsar Timing Arrays with the overlap reduction function for massive gravity one needs to look at Bayesian statistic. The underlying methods are used by the Software PTArcade [22] to calculate the probability density of the parameter m_g and thus deliver an limit for the graviton mass.

A basic concept of bayesian statistic is how probabilities should be updated when taking new information into account.

In the Bayesian framework one assumes the data d as fixed and the parameters $\vec{\theta}$ of a hypothesis $\mathcal{H}$ as randomly distributed. The data in our case is the 15-year dataset of NANOGrav[1]. It will be used to update our prior knowledge $p(\vec{\theta}, \mathcal{H})$ of the hypothesis using Bayes theorem

$$p(\vec{\theta}|d, \mathcal{H}) = \frac{p(d|\vec{\theta}, \mathcal{H})p(\vec{\theta}|, \mathcal{H})}{p(d|\mathcal{H})}. \tag{71}$$

It gives the posterior probability in terms of the prior probability, the likelihood and the marginal likelihood (often “evidence", is the likelihood integrated over the parameter space $\vec{theta}$) in the denominator[9].

The posterior probability distribution $p(\vec{\theta}|d, \mathcal{H})$ holds the probability that the set of parameters $\vec{\theta}$ for hypothesis $\mathcal{H}$ could generate the given data d. The likelihood $p(d|\vec{\theta}, \mathcal{H})$ is the probability that the dataset d is drawn from a random distribution described by $\mathcal{H}$ and parameterized by $\vec{\theta}$. Very importantly, the prior $p(\vec{\theta}, \mathcal{H})$ includes any knowledge we already have about the hypothesis.

The Markov Chain Monte Carlo (MCMC) method creates samples of parameter values directly from the posterior distribution. It begins with a random given point $\vec{x}$ in the parameter space, from where a jump proposal distribution function $q(\vec{y}|\vec{x})$ suggests a new point $\vec{y}$. MCMC algorithm generated points are always just dependent on their precedator (defining for the Markov Chain method) and are not independent like in other Monte Carlo methods. If a next point increases the the evaluated posterior at this new point, here, the probability distribution, it is accepted. The probability for an acception is $\alpha = \min(1, \mathrm{HST})$ with

$$\mathrm{HST}_{\vec{x}\to\vec{y}} = \frac{p(\vec{y}|d)q(\vec{x}\vec{y})}{p(\vec{x}|d)q(\vec{y}\vec{x})} \tag{72}$$

the Hastings ratio, as known from the Metropolis-Hastings-Algorithm.

This is repeated for many iterations until a convergence criterium is reached[9]. Like this a *chain* of correlated parameter values is created over n iterations, improving the aproximation

of the posterior. The parameter space $\vec{\theta}$ that is to be explored, consists of the graviton mass, the amplitude (logarithmic) and the spectral index ($\log_{10} m_g, \log_{10} A_{\mathrm{GW}}, \gamma_{\mathrm{GW}}$) but also of the parameters individually describing each pulsar's red-noise, as elaborated in the following section.

4.2 NANOGrav - Pulsar Timing Arrays

In June 2023 the dataset [1] of the North American Nanohertz Observatory for Gravitational Waves (NANOGrav) has unveiled a strong evidence for the SGWB[3]. Collecting data from 68 pulsars for over 15 years enables an analysis of the data looking at modified gravitational theories (see Fig.3 for an illustration of PTA measurement).

Figure 3: Artistic visualization of the NANOGrav Pulsar overservation. Different radiotelescopes on earth observe the behaviour of pulsars to learn more about gravitational background and its sources. Here supermassive black holes are shown as a source for these space-time perturbations. However, there are also other theories e.g. on early universe phase transitions [4, 11]. Illustration from [25].

The pulsars in the array are millisecond pulsars that have very stable rotational periods and a frequency accuracy up to 10^{-14} Hz making them ideal time-takers. High energy particles in the their magnetosphere excite beams of radiation. The ionized stellar medium (ISM) through which the radio signal passes, causes lower frequencies to arrive later at the telescope. Therefore the signal has to be dedispersed (e.g. by convolving with the inverse transfer function of the ISM). To increase the signal to noise ratio and receive a stable train of pulses, the pulse shapes are being averaged over brief observing windows ($\sim$ minutes to hours). The shape of each pulse from one rotation varies randomly, but averaged, they are remarkably stable [24, 27]. After creating pulse files, the times of arrival (TOA) are obtained by measuring the time shift of the observed profile relative to a model for each pulsar, known as a template. The timing model used by [1] to describe each pulsars behavior constists of six categories: The *spin* (describing phase, frequency and frequency derivative), *astrometry* (pulsar's position in elliptic coordinates, proper

motion and parallax), *binary* (for fifty pulsars the orbit with a companion star is modelled, see page 50 of [1]), *dispersion measure* (differences in the signal's passing-section of the solar winds and integrated density of free electrons in the line of sight which broaden the pulses frequency-wise), *frequency dependence* (additional time-independent but frequency-dependent delays for each pulsar) and lastly *jumps* (for unknown phase-offsets between different telescopes).
Subtracting the expected arrival times from the actual arrival times results in timing residuals. Of course these residuals still contain inaccuracies. There are general measuring uncertainties, uncorrelated in time, e.g. from the actual arrival times, modelled as gaussian *white noise*. The second type of uncertainty is *red-noise*, which is long-timescale correlated data ($\sim \mathrm{yr}^{-1}$). The nanohertz GWs are actually part of red-noise which is common to all pulsars, but there further is pulsar intrinsic red noise (stationary and gaussian) which is individually modelled by a power law for each pulsar (Section three of [13], [7])

$$P(f) = A_{\mathrm{red}}^2 \left(\frac{f}{1\mathrm{yr}^{-1}}\right)^{\gamma_{\mathrm{red}}}. \tag{73}$$

4.3 Implementation in PTArcade

The parameters we are surveilling in the fitting process are the graviton mass $[m_g]= \mathrm{eV}/c^2$, the amplitude of the SGWB power-law A_{gw} and its spectral index γ_{gw}. The Listing 1 shows the model-file for the implementation of cross power spectral density in `PTArcade`[22], a software to fit models to a PTA dataset by MCMC-sampling. Firstly the `Uniform` prior probability distributions are set for wanted parameters from line 10 to 14 and in a seperate configuration file the mode "`enterprise`" is chosen, describing the likelihood function $p(\vec{\delta t})$ for pulsar timing residuals $\vec{\delta t}$ as [23]

$$p(\vec{\delta t}) = \frac{\exp(-\frac{1}{2}\vec{\delta t}^T \mathbf{C}^{-1} \vec{\delta t})}{\sqrt{\det(2\pi\mathbf{C})}}. \tag{74}$$

The likelihood is solely dependent on the parameters $\vec{\theta}$ which describe the red-noise covariance matrix. The composition of $\mathbf{C}$ is explained in [12, 23].

The ORF $\Gamma_{ab}(\xi_{ab}, f)$ is split into more simple parts, like in Eq. 66. For a separation angle of $\xi = 0$ (`pos1 = pos2`) the autocorrelation function is used in the model-file.

In order to include the signal of our model in the code-file, we derive the expression for the GW energy density Ω_{GW}.

The ORF for massive gravity $\Gamma_{ab}(\xi_{ab}, f)$ is part of the cross-power spectrum

$$S_{ab}^{\mathrm{GW}}(f) = \Gamma_{ab}\frac{S_h(f)}{4\pi^2 f^2} \tag{75}$$

where $S_h(f)$ is the GW strain power spectrum. It is related to the characteristic GW strain amplitude $h_c(f)$ by

$$h_c(f) = \sqrt{2fS_h(f)}. \tag{76}$$

and to the GW energy density spectrum (GW energy density power spectrum in units of the total density of the Universe)[20] by

$$\Omega_{\mathrm{GW}} = \frac{4\pi^2}{3H_0^2}f^3 S_h(f) \tag{77}$$

Choosing a power law ansatz for h_c results in the timing-residual cross-power spectral density becoming[2]

$$S_{ab}^{\mathrm{GW}}(f) = \Gamma_{ab}\frac{A^2}{12\pi^2 f_{yr}^3}\left(\frac{f}{f_{yr}}\right)^{-\gamma}, \tag{78}$$

with Γ_{ab} as the spatial correlation function. Then the GW energy density is

$$\Omega_{\mathrm{GW}} = \frac{2\pi^2 A^2}{3H_0^2}f_{yr}^2\left(\frac{f}{f_{yr}}\right)^{5-\gamma}. \tag{79}$$

The code file, Listing 1, uses $h^2\Omega_{\mathrm{GW}}$, as required by `PTArcade` [23], because it is independent of the precise value of the Hubble constant H_0. h is a dimensionless constant, coming from the expression $H_0 = 100\,h\,\mathrm{kms}^{-1}\mathrm{Mpc}^{-1}$. Like this the `spectrum` is defined as

$$\Omega = \frac{2\pi^2}{3}A^2 f_{yr}^2\left(\frac{h}{H_0}\right)^2\left(\frac{f}{f_{yr}}\right)^{5-\gamma}. \tag{80}$$

```
1    import numpy as np
2        import ptarcade.models_utils as aux
3        from ptarcade.models_utils import prior
4        from enterprise import constants as const
5
6        name = "massive_gr"
7
8        smbhb = False
```

```
        # priors of the parameters
        parameters = {
            "log10_mg": prior("Uniform", -26, -20),
            "log10_A": prior("Uniform", -18, -11),
            "gamma": prior("Uniform", 0, 7)
        }
        # group velocity k/k0
        def v_g(f, mg):
            return np.sqrt((2 * np.pi * f)**2 - mg**2) / (2 * np.pi * f)
        # parts of the ORF as in (66)
        def X(v_gr, cos_ab):
            return -10 * v_gr**3 * cos_ab + 12 * v_gr * cos_ab + 6 * v_gr

        def Y(v_gr, cos_ab):
            return -6 * (1 + cos_ab - v_gr**2 * (3 * cos_ab - 1))

        def Z(v_gr, cos_ab):
            num = -3 * (1 + 2 * v_gr**2 * (1 - 2 * cos_ab) - v_gr**4
            * (1 - 2 * cos_ab**2))
            den = np.sqrt((1 - cos_ab) * (2 - v_gr**2 * (1 + cos_ab)))
            return num / den

        def Q(v_gr, cos_ab):
            num = (1 + 2 * v_gr**2 * (1 - 2 * cos_ab) - v_gr**4 *
            (1 - 2 * cos_ab**2) - 2 * v_gr * (1 - v_gr**2 * cos_ab) *
            np.sqrt((1 - cos_ab) * (2 - v_gr**2 * (1 + cos_ab))))
            den = (v_gr**2 - 1)**2
            return num / den

        def orf(f, pos1, pos2, log10_mg, log10_A, gamma):
            mg = 10 ** (log10_mg - 9) * aux.gev_to_hz
            f_g = mg / (2*np.pi)
            cos_ab = np.dot(pos1, pos2)
            v_gr = v_g(f, mg)

            if np.all(pos1 == pos2):
                # Implementing \Gamma_{aa}(f)
                return np.array([1 / (2 * v_g(fi, mg)**5)
                *(6 * v_g(fi, mg) - 4 * v_g(fi, mg)**3 + 3
                *(v_g(fi, mg)**2 - 1) * np.log((1 + v_g(fi, mg))
                /(1 - v_g(fi, mg))))
                    if fi > f_g else 0 for fi in f])
```

```
            else:
                # Implementing \Gamma_{ab}(f)
                return np.array([1 / 16 / v_gr**5 * (X(v_gr, cos_ab)
                + Y(v_gr, cos_ab) * np.log((1 + v_gr) / (1 - v_gr))
                + Z(v_gr, cos_ab) * np.log(Q(v_gr, cos_ab)))
                    if fi > f_g else 0 for fi in f])

        def spectrum(f, log10_mg, log10_A, gamma):
            f_g = 10**(log10_mg - 9) * aux.gev_to_hz / (2*np.pi)
            return np.array([2*np.pi**2/3 *(aux.h/aux.H_0_Hz)**2
            *(10 ** log10_A)** 2 * const.fyr**2 *
            (fi/const.fyr)**(5 - gamma) if fi > f_g else 0 for fi in f])


```

Listing 1: Python implementation of the timing-residual cross-power spectral density

In combination with a configuration file this poses the input for `PTArcade` (see [22]). The output is in the form of Markov Chains that can then be used to derive posterior destributions for the parameters that are of interest [21, 23].

5 Results and Discussion

To present the posterior functions of multiple parameters a cornerplot is used. As seen below, Fig. 4 shows the 1- and 2D posterior distributions for the three main parameters, including the graviton mass. The light- and darkblue shaded regions and the dashed lines in the cornerplot mark the Bayesian credible regions and intervals in the posterior distributions. The Bayesian credible regions marked by the dashed lines are defined as the highest-posterior-density intervals (HPDIs) These are determined by integrating over the regions of highest posterior density until it yields an integrated probability of 68% or 95%. The values of the GW power-law parameters (A and γ) show a fairly symmetric 1D distribution and have stable 2D distributions for low values of m_g. Their maximal posterior value is $\log A_{\max} = -14.19$ with a 1σ-HPDI between $[-14.34, -14.06]$ and $\gamma_{\max} = 3.27$ in the 1σ interval of $[2.92, 3.67]$. The three panels below the diagonal show the 2D posterior distribution for the A_{GW} and γ_{GW} parameters in relation to m_g and to each other.

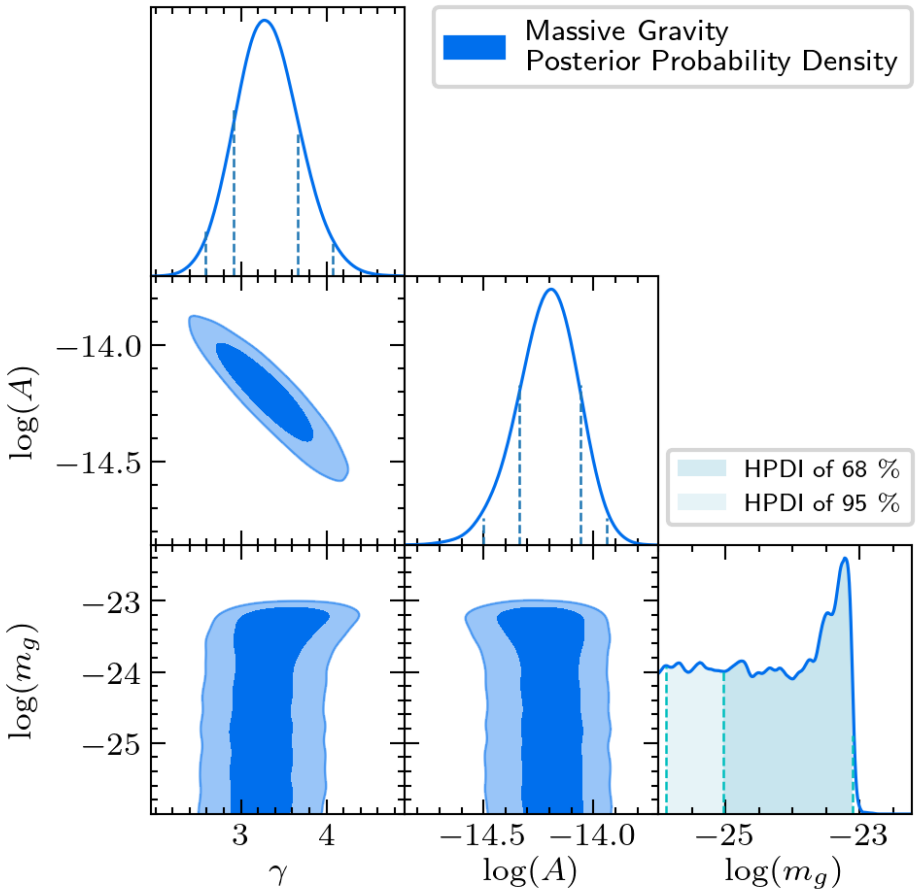

Figure 4: Cornerplot of marginalized posterior distributions for the parameters $\log(A), \gamma$ and $\log(m_g)$ derived from Markov Chains. The diagonal of the cornerplot shows the 1D posteriors while the three other plots show a posterior distribution of two of the parameters. The two blue-shaded regions show the 68% and 95% confidence intervals. The HPDIs of the same value are shown by the vertical dashed lines. For the 1D-plot of m_g the upper limit of both HPDIs are not graphically distiguishable. Analysis tools from `PTArcade`[21].

The most relevant graph for this analysis is in the lower right corner. It shows the probabilty density of values for the graviton mass. As caused by the steep decline of the posterior the upper limit of the HPDIs coincide in this panel. One can see that the posterior is settling into a constant for lower values of $\log m_g$. Apart from a small stochastic variations (The bandwidth for the Kernel Density Estimation (KDE) can vary this) the probabiltity stays in a small range of probabilty as it goes towards zero. This means that for v_{gr} approaching the speed of light, the Hellings Downs correlation is not effected and does not deviate from the GR-based form. The altered dispersion relation used in the ORF only starts to have a relevant influence when m_g becomes larger than $m_g > 10^{-24}\,\text{eV}$. The data suggests that values of m_g between 10^{-23} and $10^{-24}\,\text{eV}$ are more probabable than lower values. As visible in Figure 4 the probability density for the parameter starts to strongly increase and reaches a peak at $m_{g,\max} = 6.00 \times 10^{-24}\,\text{eV}$.

The Bayes Estimator (BE) lies at $m_{g,\,\mathrm{BE}} = (3.63 \pm 7.57) \times 10^{-25}\,\mathrm{eV}$, as the plateau pulls the mean towards a lower value.
Nonetheless, this does not rule out the possibility of a massless graviton. Just because the influence of the hypothesis on the ORF does not stand out for lower graviton masses does not mean they are ruled out.
The conclusion is that the data is able to constrain the graviton mass from above. It enables setting a reliable boundary, disqualifiying masses above a certain value.
The 95%-HPDI upper limit is reached for $m_{g,\,95\%} = 7.82 \times 10^{-24}\,\mathrm{eV}$. This means that with an almost certain probability m_g lies below this value and is thus the concluded limit from this analysis.

A more conservative way of constrainment can be considered as well, when looking for the value at which the probability density for m_g has dropped to 10% of the averaged plateau-value. This leads to a boudary value of $m_{g,\mathrm{conserv.}} = 1.07 \times 10^{-23}\,\mathrm{eV}$.

6 Outlook

Using the framework of PTA analysis, the GW propagation speed v_{gr} was examined. After giving a comprehensive and more detailled course of the analytic calculation of the ORF in Chapter 3, an improved version of the ORF was implemented. Using the precise approximation of the autocorrelation coefficient[8] and the statistic tools of PTArcade, a reliable basis to constrain the parameter of m_g was built.
The ORF calculation can be extended by including other characteristic aspects that follow when assuming a mass. In this thesis only the tensor modes ($\pm$2-spin polarizations) were considered, but also vector- and skalar modes play a role[19], as well as longitudal spacetime perturbations as opposed to only perpendicular to the propagation direction.
Utilizing the PTArcade evaluation tools the 95%-HPDI upper limit is reached for $m_{g,\,95\%} = 7.82 \times 10^{-24}\,\mathrm{eV}$. Taking a more conservative bound from the posterior distribution, one can make sure not to exclude values prematurely. It was achieved by using the average plateau-value as a reference, where m_g is too small to show an effect in the data, and setting the point of constraint to when the function has dropped to 10% of this plateau. This leads to $m_g \lesssim 1.07 \times 10^{-23}\,\mathrm{eV}$. Regarding the future, the total observation time T_{obs} will further increase as NANOGrav continues its PTA-projects. It is currently moving from 2 nHz (15 years of observation) towards 1 nHz (30 years of observation). The smallest frequency bin will steadily decrease. The compton frequency which a massive graviton inherently has, $f_g = m_g/2\pi$, and

its associated cut-off (around $\sim 10^{-23}\,\mathrm{eV}$) will be lowered with time.

It can further be interesting investigating the origin of the SGWB and whether other sources, like ultralight dark matter [28], can leave GW-like imprints on PTA data.

Improvements on the timing models, the incorporation of theoretical uncertainties the inclusion of new pulsars will also strengthen the derived results. It would further be interesting to see other PTA data sets being used to test modified gravity theories in PTArcade, as well as combined sets, like (international) IPTA.

APPENDIX A: Hellings-Downs-curve in GR

Simplification of the Hellings and Downs curve integral

In the following, Eq.19 will be simplified to the point of Eq. 24, as seen in [16].

$$
\begin{aligned}
C(\xi) &= \frac{1}{4\pi}\int \mathrm{d}^2\vec{k}\; F_a^A(\vec{k})F_b^A(\vec{k}) && \text{(A.1)}\\
&= \frac{1}{16\pi}\int \mathrm{d}^2\vec{k}\; \frac{n_a^i n_a^j e_{ij}^+(\vec{k})\cdot\; n_b^k n_b^l e_{ij}^+(\vec{k})}{(1+\vec{k}\cdot\vec{n}_a)(1+\vec{k}\cdot\vec{n}_b)}\\
&= \frac{1}{16\pi}\int \mathrm{d}^2\vec{k}\;\cdot \frac{\sin^2\theta}{(1+\cos\theta)}\frac{(\sin\xi\cos\theta\cos\phi-\cos\xi\sin\theta)^2-\sin^2\xi\sin^2\phi}{(1+\cos\xi\cos\theta+\sin\xi\sin\theta\cos\phi)}\\
&= \frac{1}{16\pi}\int_0^\pi \mathrm{d}\cos\theta(1-\cos\theta)\cdot I(\cos\theta,\xi) && \text{(A.2)}
\end{aligned}
$$

defining

$$
I(\cos\theta,\xi) \equiv \int_0^{2\pi}\mathrm{d}\phi\frac{1}{2}\frac{(\sin\xi\cos\theta\cos\phi-\cos\xi\sin\theta)^2-\sin^2\xi\sin^2\phi}{(1+\cos\xi\cos\theta+\sin\xi\sin\theta\cos\phi)}. \tag{A.3}
$$

As to be shown the integral $I(\cos\theta,\xi)$ can be expressed as $I=\int_0^{2\pi}\mathrm{d}\phi F_2^+(\vec{k})$, where

$$
F_2^+(\vec{k}) = \frac{1}{2}\left[(1-\cos\xi\cos\theta-\sin\xi\sin\theta\cos\phi)-\frac{2\sin^2\xi\sin^2\phi}{1+\cos\xi\cos\theta+\sin\xi\sin\theta\cos\phi}\right]. \tag{A.4}
$$

Defining $a\equiv(\cos\xi\cos\theta)$ and $b\equiv(\sin\xi\sin\theta\cos\phi)$ one can factor the integrand of I as

$$
\begin{aligned}
I &= \frac{1}{2}\int_0^{2\pi}\mathrm{d}\phi\frac{(1-a-b)(a^2-2ab+b^2-\sin^2\xi\sin^2\phi)}{(1+a+b)(1-a-b)} && \text{(A.5)}\\
&= \frac{1}{2}\int_0^{2\pi}\mathrm{d}\phi(1-a-b)\left[\frac{a^2-2ab+b^2+\sin^2\xi\sin^2\phi}{(1+a+b)(1-a-b)}\right] && \text{(A.6)}\\
&\quad + \frac{(-\sin^2\xi\sin^2\phi-\sin^2\xi\sin^2\phi)(1-a-b)}{(1+a+b)(1-a-b)}\\
&= \frac{1}{2}\int_0^{2\pi}\mathrm{d}\phi\frac{1}{2}(1-a-b)-\frac{1}{2}\int_0^{2\pi}\mathrm{d}\phi\frac{2\sin^2\xi\sin^2\phi}{(1+a+b)} && \text{(A.7)}\\
&= \int_0^{2\pi}\mathrm{d}\phi F_2^+(\vec{k}) \equiv I_1 - I_2 && \text{(A.8)}
\end{aligned}
$$

The term in angled brackets (Eq.A.6 equals to one:

$$\begin{aligned}
&\frac{a^2 - 2ab + b^2 + \sin^2\xi \sin^2\phi}{1 - a^2 - 2ab - b^2} = 1 \\
\Leftrightarrow\ & x^2 \sin^2\xi \cos^2\phi + \cos^2\xi \sin^2\theta = 1 - x^2\cos^2\xi - \sin^2\xi(1-x^2)\cos^2\phi \\
\Leftrightarrow\ & \cos^2\xi - x^2\cos^2\xi + \sin^2\xi\sin^2\phi = 1 - x^2\cos^2\xi - \sin^2\xi(1-\sin^2\phi) \\
\Leftrightarrow\ & \cos^2\xi + \sin^2\xi\sin^2\phi = 1 - \sin^2\xi + \sin^2\xi\sin^2\phi \\
\Leftrightarrow\ & \cos^2\xi = \cos^2\xi, \qquad \text{where} \quad x \equiv \cos\theta.
\end{aligned}$$

So eventually

$$C(\xi) = \frac{1}{16\pi}\int_0^\pi \mathrm{d}\cos\theta\ \ (1-\cos\theta)\cdot\int_0^{2\pi}\mathrm{d}\phi F_2^+(\vec{k}). \tag{A.9}$$

Calculation of the Integral I_2 with contour integration

The steps leading to the result in Eq.26 are shown below.

$$I_2 = -\frac{1}{2}\int_0^{2\pi}\mathrm{d}\phi\frac{2\sin^2\xi\sin^2\phi}{(1+\cos\xi x + \sin\xi\sqrt{1-x^2}\cos\phi)} = -\sin^2\xi\int_0^{2\pi}\mathrm{d}\phi f(z) \tag{A.10}$$

The contour integral takes place in the positive complex plane so we are introducing $z = e^{i\phi}$, $dz/d\phi = iz$, $\cos\phi = \frac{1}{2}(z+\frac{1}{z})$ and $\sin\phi = \frac{1}{2i}(z+\frac{1}{z})$. Extending with z/z and noting that $z(z-1/z)^2 = (z^2-1)^2/z$ results in

$$f(z) = \frac{i(z-\frac{1}{z})^2}{z^2\left[4z(1+\cos\xi x) + 2\sqrt{1-x^2}\sin\xi(z^2+1)\right]}.$$

This function has poles. The obvious one is a double pole and lies at $z = 0$. As seen in [16] the term in angled brackets in the denominator can be factorized

$$\begin{aligned}
&4z(1+x\cos\xi) + 2\sqrt{1-x^2}\sin\xi(z^2+1) \stackrel{!}{=} 2\sqrt{1-x^2}\sin\xi\,(z-z_+)\,(z-z_-) \\
&= 2\sqrt{1-x^2}\sin\xi(z^2+1) + 2\sqrt{1-x^2}\sin\xi\cdot z\frac{2(1+x\cos\xi)}{\sqrt{1-\cos^2\xi}\sqrt{1-x^2}} \\
&= 4z(1+x\cos\xi) + 2\sqrt{1-x^2}\sin\xi(z^2+1)
\end{aligned}$$

to single out the other poles which are stated as

$$z_+ \equiv -\sqrt{\left(\frac{1\mp\cos\xi}{1\pm\cos\xi}\right)\left(\frac{1\mp x}{1\pm x}\right)}, \quad z_- \equiv \frac{1}{z_+}. \tag{A.11}$$

As z_- is not inside the unitcircle [3] it does not contribute to the sum over the residues. Hence we have

$$\mathrm{Res}(f, z_+) = \lim_{z \to z_+} \left[(z - z_+) \cdot f(z) \right]$$

$(z - z_+)$ cancels with a denominator factor in $f(z)$ and we can perform the limes:

$$\mathrm{Res}(f, z_+) = \frac{i(z_+ - z_-)}{2\sqrt{1 - x^2}\sin\xi}.$$

Further the residue of the pole of second order is calculated:

$$\mathrm{Res}(f, 0) = \lim_{z \to 0} \left[\frac{\mathrm{d}}{\mathrm{d}z} (z^2 f(z)) \right] = \frac{i(z_+ - z_-)}{2\sqrt{1 - x^2}\sin\xi}$$

According to the residue theorem for a trigonometric function[6] the integral is then given by

$$\oint_{\text{unitcircle}} f(z)dz = 2\pi i \left[\mathrm{Res}(z_+) + \mathrm{Res}(z_0) \right] = -2\pi \frac{z_+}{\sqrt{1 - x^2}\sin\xi} \tag{A.12}$$

Seperatly looking at the signs and using $\sin\xi = (1 + \cos\xi)(1 - \cos\xi)$, according to the notation of Eq.A.10 the integral I_2 is then

$$I_2 = \frac{-2\pi \sin^2\xi}{(1 \pm x)(1 \pm \cos\xi)} = \frac{-2\pi(1 \mp \cos\xi)}{(1 \pm x)}. \tag{A.13}$$

[3] Pole z_- does not lie inside the unit circle: $|z_+| \leq 1 \longleftrightarrow |1/z_-| \leq 1 \Longrightarrow |z_-| \geq 1$

References

[1]G. Agazie, M. F. Alam, A. Anumarlapudi, A. M. Archibald, Z. Arzoumanian, P. T. Baker, L. Blecha, V. Bonidie, A. Brazier, P. R. Brook, et al., "The nanograv 15 yr data set: observations and timing of 68 millisecond pulsars", The Astrophysical Journal Letters **951**, L9 (2023).

[2]G. Agazie, A. Anumarlapudi, A. M. Archibald, Z. Arzoumanian, J. G. Baier, P. T. Baker, B. Bécsy, L. Blecha, A. Brazier, P. R. Brook, et al., "The nanograv 15 yr data set: running of the spectral index", arXiv preprint arXiv:2408.10166 (2024).

[3]G. Agazie, A. Anumarlapudi, A. M. Archibald, Z. Arzoumanian, P. T. Baker, B. Bécsy, L. Blecha, A. Brazier, P. R. Brook, S. Burke-Spolaor, et al., "The nanograv 15 yr data set: evidence for a gravitational-wave background", The Astrophysical Journal Letters **951**, L8 (2023).

[4]P. Auclair, S. Blasi, V. Brdar, and K. Schmitz, "Gravitational waves from current-carrying cosmic strings", Journal of Cosmology and Astroparticle Physics **2023**, 009 (2023).

[5]R. C. Bernardo and K.-W. Ng, "Constraining gravitational wave propagation using pulsar timing array correlations", Physical Review D **107**, L101502 (2023).

[6]M. L. Boas, *Mathematical methods in the physical sciences* (John Wiley & Sons, 2006).

[7]S. J. Chamberlin, J. D. Creighton, X. Siemens, P. Demorest, J. Ellis, L. R. Price, and J. D. Romano, "Time-domain implementation of the optimal cross-correlation statistic for stochastic gravitational-wave background searches in pulsar timing data", Physical Review D **91**, 044048 (2015).

[8]N. Cordes, A. Mitridate, K. Schmitz, T. Schröder, and K. Wassner, "On the overlap reduction function of pulsar timing array searches for gravitational waves in modified gravity", arXiv preprint arXiv:2407.04464 (2024).

[9]J. A. Ellis, "A bayesian analysis pipeline for continuous gw sources in the pta band", Classical and Quantum Gravity **30**, 224004 (2013).

[10]E. E. Flanagan and S. A. Hughes, "The basics of gravitational wave theory", New Journal of Physics **7**, 204 (2005).

[11]Y. Gouttenoire, S. Trifinopoulos, G. Valogiannis, and M. Vanvlasselaer, "Scrutinizing the primordial black hole interpretation of pta gravitational waves and jwst early galaxies", Physical Review D **109**, 123002 (2024).

[12]R. van Haasteren and Y. Levin, "Understanding and analysing time-correlated stochastic signals in pulsar timing", Monthly Notices of the Royal Astronomical Society **428**, 1147–1159 (2012).

[13]R. van Haasteren and M. Vallisneri, "New advances in the gaussian-process approach to pulsar-timing data analysis", Physical Review D **90**, 104012 (2014).

[14]R. Hellings and G. Downs, "Upper limits on the isotropic gravitational radiation background from pulsar timing analysis", Astrophysical Journal, Part 2-Letters to the Editor, vol. 265, Feb. 15, 1983, p. L39-L42. **265**, L39–L42 (1983).

[15]M. Isi and L. C. Stein, "Measuring stochastic gravitational-wave energy beyond general relativity", Physical Review D **98**, 104025 (2018).

[16]F. A. Jenet and J. D. Romano, *Understanding the gravitational-wave hellings and downs curve for pulsar timing arrays in terms of sound and electromagnetic waves*, 2015.

[17]K. Lee, F. A. Jenet, R. H. Price, N. Wex, and M. Kramer, "Detecting massive gravitons using pulsar timing arrays", The Astrophysical Journal **722**, 1589 (2010).

[18]Q. Liang, I. Obata, and M. Sasaki, "Testing gravity with frequency-dependent overlap reduction function in pulsar timing array", arXiv preprint arXiv:2405.11755 (2024).

[19]Q. Liang and M. Trodden, "Detecting the stochastic gravitational wave background from massive gravity with pulsar timing arrays", Physical Review D **104**, 084052 (2021).

[20]M. Maggiore, *Gravitational waves: volume 1: theory and experiments*, Gravitational Waves (OUP Oxford, 2008).

[21]A. Mitridate, "Ptarcade", `10.5281/zenodo.7876430` (2023).

[22]A. Mitridate, *New physics meets ptas*, `https://andrea-mitridate.github.io/PTArcade/` (visited on 08/16/2024).

[23]A. Mitridate, D. Wright, R. von Eckardstein, T. Schröder, J. Nay, K. Olum, K. Schmitz, and T. Trickle, "PTArcade", (2023).

[24]J. Nay, *Harmonic analysis method to search for gravitational waves with pulsar timing arrays*, `https://indico.cern.ch/event/1319151/contributions/5573980/attachments/2731752/4749109/Harmonic%20Analysis%20for%20PTAs-TACOS.pdf` (visited on 08/06/2024).

[25]O. Shmahalo, *Multimessenger astrophysics*, `https://nanograv.org/science/topics/multimessenger-astrophysics` (visited on 08/02/2024).

[26]J. Simon, N. Collaboration, et al., "The nanograv 12.5-year data set: search for an isotropic stochastic gravitational-wave background", in American astronomical society meeting abstracts, Vol. 237 (2021), pp. 335–14.

[27]S. R. Taylor, "The nanohertz gravitational wave astronomer", arXiv preprint arXiv:2105.13270 (2021).

[28]S. Wang and Z.-C. Zhao, "Unveiling the graviton mass bounds through the analysis of 2023 pulsar timing array data releases", Physical Review D **109**, L061502 (2024).

[29]Y.-M. Wu, Z.-C. Chen, Y.-C. Bi, and Q.-G. Huang, "Constraining the graviton mass with the nanograv 15 year data set", Classical and Quantum Gravity **41**, 075002 (2024).